Electronic Supplementary Material (ESI) for Dalton Transactions

Supporting Information

A Comparison of Sensitised Ln(III) Emission with Pyridine- and Pyrazine-2,6-Dicarboxylates – Part II

Evan G. Moore,*[a,c,d] Jakob Grilj,[b] Eric Vauthey,[b] and Paola Ceroni.[c]

a. School of Chemistry, University of Melbourne, Parkville, VIC, 3010, Australia.
b. Physical Chemistry Department, Sciences II, University of Geneva, 30, Quai Ernest Ansermet, CH-1211 Geneva 4, Switzerland.
c. Dipartimento di Chimica "G. Ciamician", Università di Bologna, Via Selmi 2, Bologna, 40126, Italy.
d. School of Chemistry and Molecular Biosciences, University of Queensland, St Lucia, QLD, 4072, Australia.
Fax: +61 (0) 7 3365 4273; Tel: +61 (0) 7 3365 3862
E-mail: egmoore@uq.edu.au

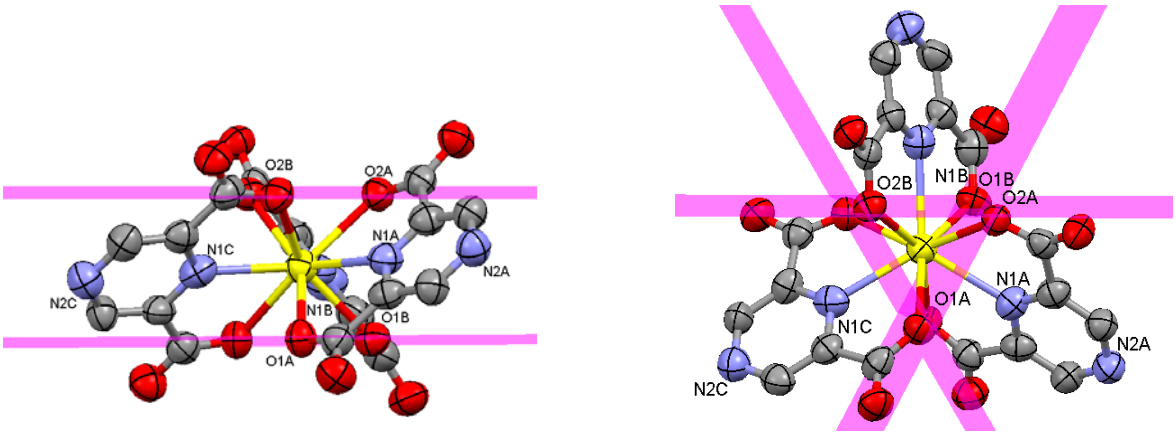

Figure S1. Additional view of X-ray crystal structure for $(Me_4N)_3[Eu(PYZ)_3].4H_2O$ showing (a) upper and lower basal planes defined by the {O1A, O1B O1C} and {O2A, O2B and O2C} atoms (left) and three lateral planes defined by {O2A, O1B, O2B, O1C}, {O1A, O2A, O1B, O2C} and {O1A, O2B, O1C, O2C} (right) (C, grey; O, red; N, blue; Eu, yellow; 50% probability ellipsoids). Me_4N^+ cations, solvent water molecules, and H atoms omitted for clarity.

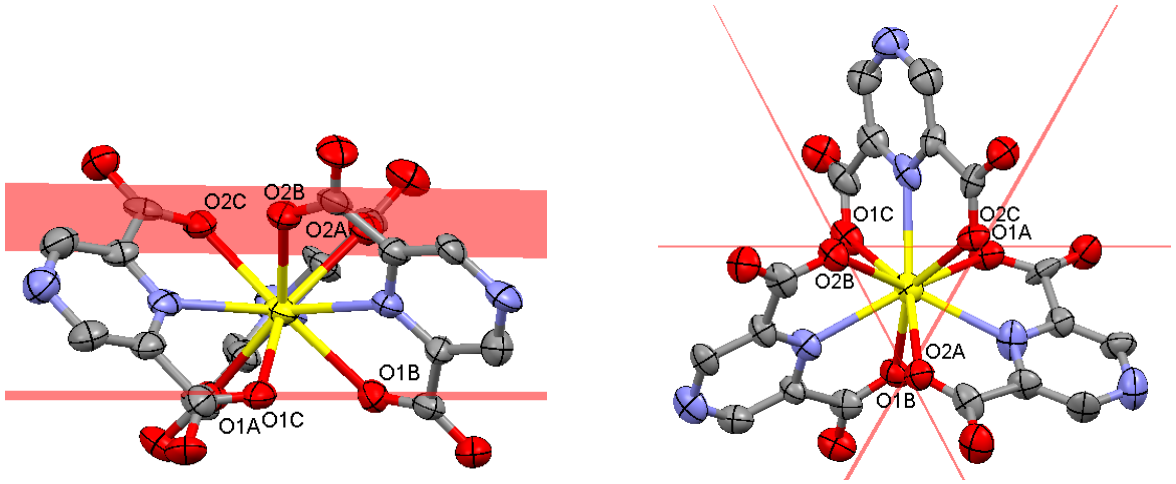

Figure S2. Additional view of X-ray crystal structure for $(Me_4N)_3[Eu(PYZ)_3].5MeOH$ showing (a) upper and lower basal planes defined by the {O1A, O1B O1C} and {O2A, O2B and O2C} atoms (left) and three lateral planes defined by {O2A, O1B, O2B, O1C}, {O1A, O2A, O1B, O2C} and {O1A, O2B, O1C, O2C} (right) (C, grey; O, red; N, blue; Eu, yellow; 50% probability ellipsoids). Me_4N^+ cations, solvent water molecules, and H atoms omitted for clarity.

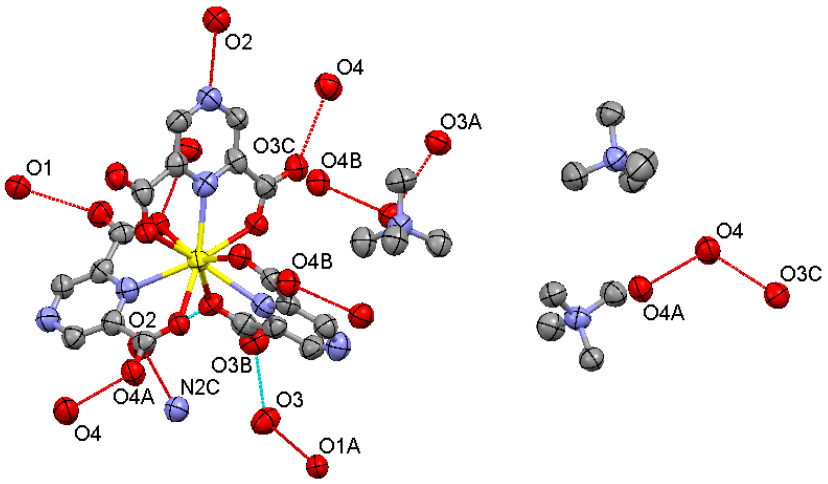

Figure S3. Additional view of X-ray crystal structure for $(Me_4N)_3[Eu(PYZ)_3].4H_2O$ showing intermolecular H-bonding interactions (C, grey; O, red; N, blue; Eu, yellow; 50% probability ellipsoids). H atoms omitted for clarity.

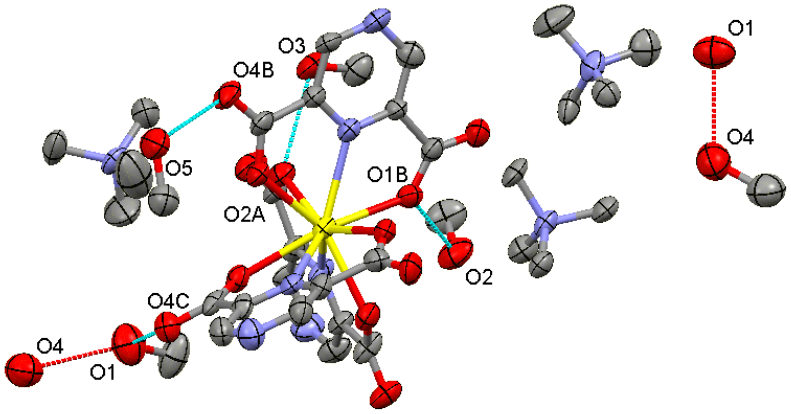

Figure S4. Additional view of X-ray crystal structure for $(Me_4N)_3[Eu(PYZ)_3].5MeOH$ showing intermolecular H-bonding interactions (C, grey; O, red; N, blue; Eu, yellow; 50% probability ellipsoids). H atoms omitted for clarity.

Table S1. List of hydrogen bonding interaction distances and angles for the $(Me_4N)_3[Eu(PYZ)_3].4H_2O$ and $(Me_4N)_3[Eu(PYZ)_3].5MeOH$ complexes.

$(Me_4N)_3[Eu(PYZ)_3].4H_2O$						
Donor (D)	H Atom (H)	Acceptor (A)	D-H (Å)	H---A (Å)	D---A (Å)	D-H---A (°)
O1	H1	O4B	0.83(9)	1.98(10)	2.805(12)	173(12)
O1	H2	O3A	0.83 (9)	2.03 (9)	2.818 (12)	158 (10)
O2	H3	O1B	0.85 (4)	2.05 (7)	2.855 (12)	158 (13)
O2	H4	N2C	0.84 (11)	2.23 (11)	3.010 (15)	154 (11)
O3	H5	O1A	0.85 (11)	2.11 (12)	2.860 (12)	147 (10)
O3	H6	O3B	0.84 (3)	2.05 (5)	2.820 (13)	152 (11)
O4	H7	O4A	0.85 (10)	1.91 (10)	2.743 (12)	167 (6)
O4	H8	O3C	0.86 (13)	1.95 (13)	2.800 (12)	174 (-1)
$(Me_4N)_3[Eu(PYZ)_3].5MeOH$						
Donor (D)	H Atom (H)	Acceptor (A)	D-H (Å)	H---A (Å)	D---A (Å)	D-H---A (°)
O1	H1	O4C	0.82	1.85	2.673 (18)	179
O2	H2	O1B	0.82	1.94	2.718 (16)	157
O5	H5	O4B	0.82	1.95	2.759 (18)	167

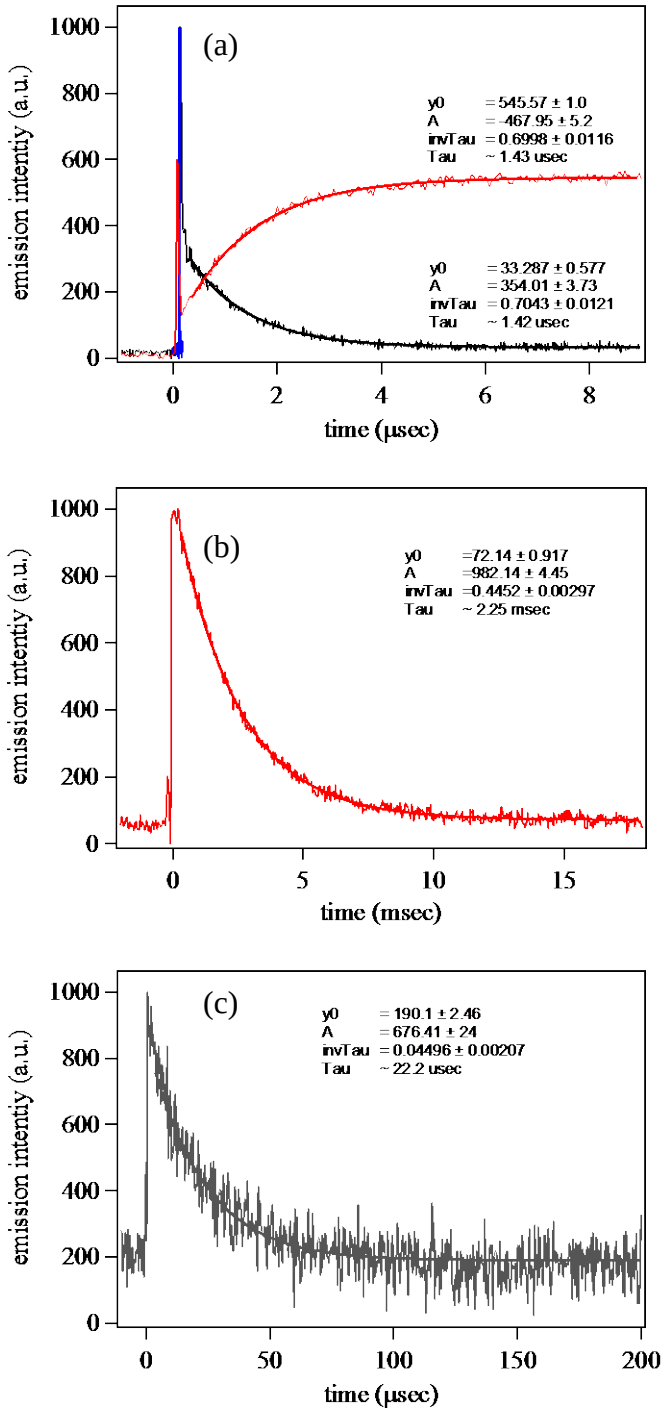

Figure S5. (a) Nanosecond laser setup instrument response function (IRF, blue, FWHM ~ 8 ns), observed decay of $^5D_1$ excited state (black, λ_{emis} = 538 nm, λ_{ex} = 280 nm) and corresponding rise (red, λ_{emis} = 615 nm, λ_{ex} = 280 nm) of the $^5D_0$ excited state for the $[Eu(DPA)_3]^{3-}$ complex. (b) Long lived decay of the $^5D_0$ excited state for the $[Eu(DPA)_3]^{3-}$ complex. (c) Decay of the $^2F_{5/2}$ excited state for the $[Yb(DPA)_3]^{3-}$ complex in the NIR region (grey, λ_{emis} = 980 nm, λ_{ex} = 266 nm).

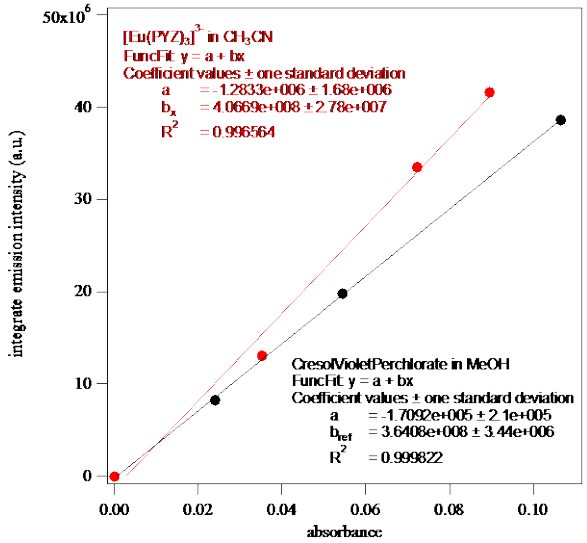

$\Phi_x = \Phi_{ref} \times (b_x/b_{ref}) \times (\eta^2_x/\eta^2_{ref})$
$= 0.54 \times (4.0669e8/3.6408e8) \times (1.3441^2/1.3280^2)$
$= 0.6179$ (~ 61.8%)

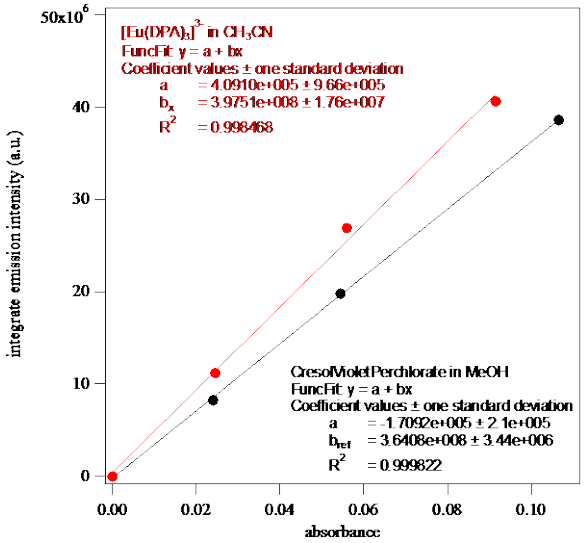

$\Phi_x = \Phi_{ref} \times (b_x/b_{ref}) \times (\eta^2_x/\eta^2_{ref})$
$= 0.54 \times (3.9751e8/3.6408e8) \times (1.3441^2/1.3280^2)$
$= 0.6039$ (~ 60.4%)

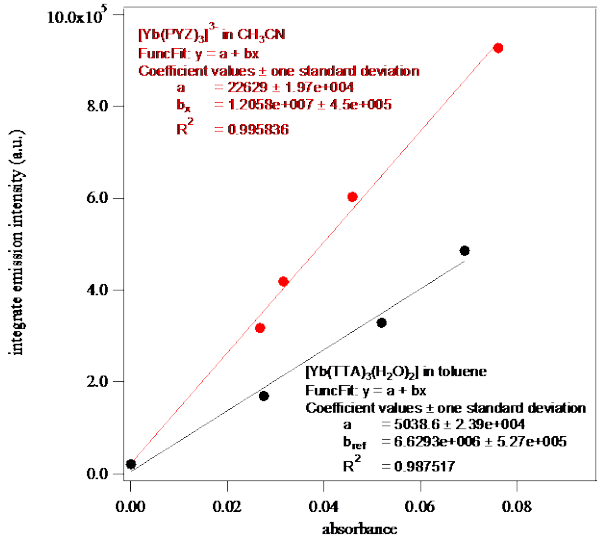

$\Phi_x = \Phi_{ref} \times (b_x/b_{ref}) \times (\eta^2_x/\eta^2_{ref})$
$= 0.0035 \times (1.2058e7/6.6293e6) \times (1.3441^2/1.4969^2)$
$= 0.00513$ (~ 0.51 %)

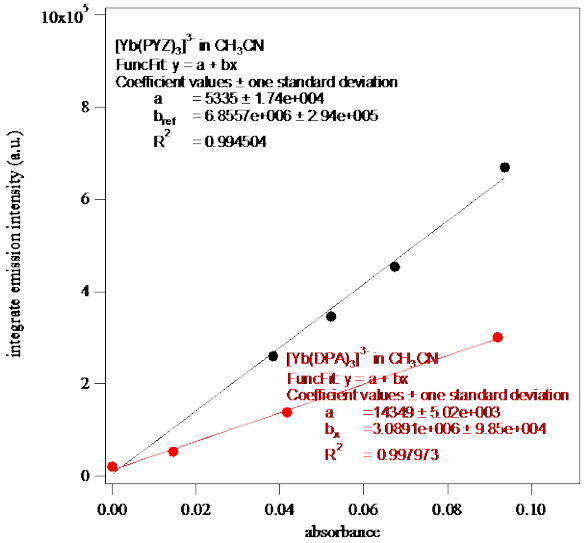

$\Phi_x = \Phi_{ref} \times (b_x/b_{ref}) \times (\eta^2_x/\eta^2_{ref})$
$= 0.00513 \times (3.0891e6/6.8557e6) \times (1.3441^2/1.3441^2)$
$= 0.00231$ (~ 0.23 %)

Figure S6. Absorption versus integrated emission plots for; **(a)** Relative quantum yield determination of $[Eu(PYZ)_3]^{3-}$ complex in CH_3CN (η = 1.3441) *vs* cresol violet perchlorate in MeOH (η = 1.3280) (λ_{ex} = 280 nm, Φ_{ref} = 54%). **(b)** Relative quantum yield determination of $[Eu(DPA)_3]^{3-}$ complex in CH_3CN (η = 1.3441) *vs* cresol violet perchlorate in MeOH (η = 1.3280) (λ_{ex} = 280 nm, Φ_{ref} = 54%). **(c)** Relative quantum yield determination of $[Yb(PYZ)_3]^{3-}$ complex in CH_3CN (η = 1.3441) *vs* $[Yb(TTA)_3(H_2O)_2]$ in toluene (η = 1.4969) (λ_{ex} = 330 nm, Φ_{ref} = 0.35%). **(d)** Relative quantum yield determination of $[Yb(DPA)_3]^{3-}$ complex in CH_3CN (η = 1.3441) *vs* $[Yb(PYZ)_3]^{3-}$ complex in CH_3CN (η = 1.3441) (λ_{ex} = 280 nm, Φ_{ref} = 0.513%).

Table S2A. Final Coordinates for $[Y(PYZ)_3]^{3-}$ from TD-DFT (B3LYP/LANL2DZ) calculations.

Atom	x	y	z
C,	-2.1823453111,	-1.7767712063,	1.8598399613
C,	2.4973817968,	1.777519627 3,	-1.4090623041
O,	3.4480786399,	2.5994457189,	-1.6320036277
O,	1.8210653884,	1.5880567431,	-0.3152366942
O,	-2.7190455969,	-2.5987257094,	2.6756011709
O,	-0.9571125619,	-2.5971973144,	-3.6949012092
O,	3.6763560309,	-2.6001755785,	1.0184252305
C,	-0.0279030132,	1.7763927589,	2.8682175624
C,	-2.4700760163,	1.7771265434,	-1.4581042052
C,	1.1772285517,	0.856310572,	3.0722957791
C,	2.0719979864,	0.8581227405,	-2.5555467421
O,	-0.6378474624,	1.5874749008,	1.7359738435
O,	-0.3091600054,	2.5983407221,	3.803329282
O,	-3.1394037028,	2.5981243927,	-2.1702418538
C,	1.9899410482,	0.851178475,	4.2243378228
O,	-1.1845033713,	1.588274276,	-1.4200636387
C,	2.6630244663,	0.8540514194,	-3.8354657147
C,	1.2374616613,	-0.8512691519,	-4.5029839087
C,	0.6336473458,	-0.8562188456,	-3.229024874
N,	1.0664319693,	0.0007308411,	-2.2802070984
H,	3.4692411719,	1.5442179236,	-4.0558724931
H,	0.8901085314,	-1.541161537,	-5.2633979659
C,	-3.2494738643,	0.8570497112,	-0.5164402127
C,	-4.6533944617,	0.8523213646,	-0.3878226292
C,	-4.5173850669,	-0.8529090095,	1.180482607
C,	-3.1122648463,	-0.8572264312,	1.0658913828
N,	-2.5076066306,	-0.0000016253,	0.2163843701
H,	-5.0017864203,	-1.5429426574,	1.8617267826
H,	-5.247726902,	1.5423511771,	-0.9755811122
C,	3.2796826242,	-0.8546573516,	3.3231221542
C,	2.478662491,	-0.858295984,	2.162911813
N,	1.4411485668,	-0.0005994767,	2.0633085436
H,	1.7777902114,	1.5410984526,	5.032951902
H,	4.1114141955,	-1.5451758197,	3.4023120706
Y,	0.0000641026,	0.0002223802,	-0.0003171163
N,	3.0433487305,	-0.002079891,	4.3590154611
N,	-5.2964239594,	-0.000412712,	0.4578780524
N,	2.2526426275,	0.0016584884,	-4.8156732785

Table S2B. Summary of excitation energies and oscillator strengths for $[Y(PYZ)_3]^{3-}$ from TD-DFT (B3LYP/LANL2DZ) calculations.

Excited State 1:	Triplet-A	2.8630 eV	433.06 nm	f=0.0000	
112 ->136	0.1044	2%			
124 ->136	-0.12343	3%			
128 ->134	0.1753	6%			
128 ->135	0.10487	2%			
128 ->136	0.13093	3%			
129 ->134	0.1055	2%			
129 ->135	-0.17204	6%			
129 ->136	0.2178	9%			
131 ->139	0.1266	3%			
132 ->134	0.23187	11%			
132 ->135	0.36658	27%			
Excited State 2:	Triplet-A	2.8631 eV	433.04 nm	f=0.0000	
111 ->136	0.1032	2%			
123 ->136	0.12241	3%			
128 ->134	-0.10387	2%			
128 ->135	0.17667	6%			
128 ->136	0.21625	9%			
129 ->134	0.17681	6%			
129 ->135	0.10336	2%			
129 ->136	-0.13179	3%			
130 ->138	-0.12286	3%			
132 ->134	0.36401	27%			
132 ->135	-0.23134	11%			
Excited State 3:	Triplet-A	2.8790 eV	430.66 nm	f=0.0000	
110 ->136	0.10114	2%			
111 ->134	0.12866	3%			
112 ->135	0.12894	3%			
123 ->134	0.16017	5%			
124 ->135	-0.16002	5%			
128 ->134	0.31673	20%			
129 ->135	0.31595	20%			
130 ->137	0.1169 3%				
132 ->136	0.3687 27%				
Excited State 4:	Triplet-A	3.0125 eV	411.57 nm	f=0.0000	
128 ->137	0.14754	4%			
129 ->138	-0.12495	3%			
130 ->134	0.37966	29%			
131 ->135	0.39797	32%			
132 ->139	0.17024	6%			
133 ->136	-0.27247	15%			
Excited State 5:	Triplet-A	3.0155 eV	411.15 nm	f=0.0000	
127 ->139	0.10172	2%			
128 ->137	-0.10887	2%			

129 ->139	-0.16829	6%
130 ->134	-0.24344	12%
130 ->135	-0.10071	2%
131 ->134	-0.1115	2%
131 ->135	0.20628	9%
131 ->136	-0.28457	16%
132 ->137	-0.11866	3%
132 ->138	0.12502	3%
133 ->134	0.13182	3%
133 ->135	0.35992	26%

Excited State 1: Singlet-A 3.2084 eV 386.44 nm f=0.0012

128 ->136	0.1273	3%
130 ->134	-0.23155	11%
131 ->135	0.33546	23%
131 ->136	-0.24696	12%
132 ->134	0.23475	11%
133 ->135	0.36267	26%

Excited State 2: Singlet-A 3.2086 eV 386.41 nm f=0.0011

129 ->136	-0.12833	3%
130 ->135	-0.28404	16%
130 ->136	-0.24025	12%
131 ->134	-0.31368	20%
132 ->135	-0.23249	11%
133 ->134	0.32596	21%

Excited State 3: Singlet-A 3.2091 eV 386.35 nm f=0.0001

130 ->134	0.45157	41%
131 ->135	0.36588	27%
133 ->136	-0.28955	17%

Excited State 4: Singlet-A 3.2235 eV 384.63 nm f=0.0016

128 ->134	0.21736	9%
129 ->135	-0.21535	9%
129 ->136	0.20101	8%
130 ->136	-0.19971	8%
131 ->139	0.11783	3%
132 ->135	0.40538	33%
133 ->134	0.22791	10%

Excited State 5: Singlet-A 3.2237 eV 384.61 nm f=0.0016

128 ->135	0.21927	10%
128 ->136	0.20057	8%
129 ->134	0.22055	10%
130 ->138	-0.11159	2%
131 ->136	0.19778	8%
132 ->134	0.40315	33%
133 ->135	-0.23093	11%

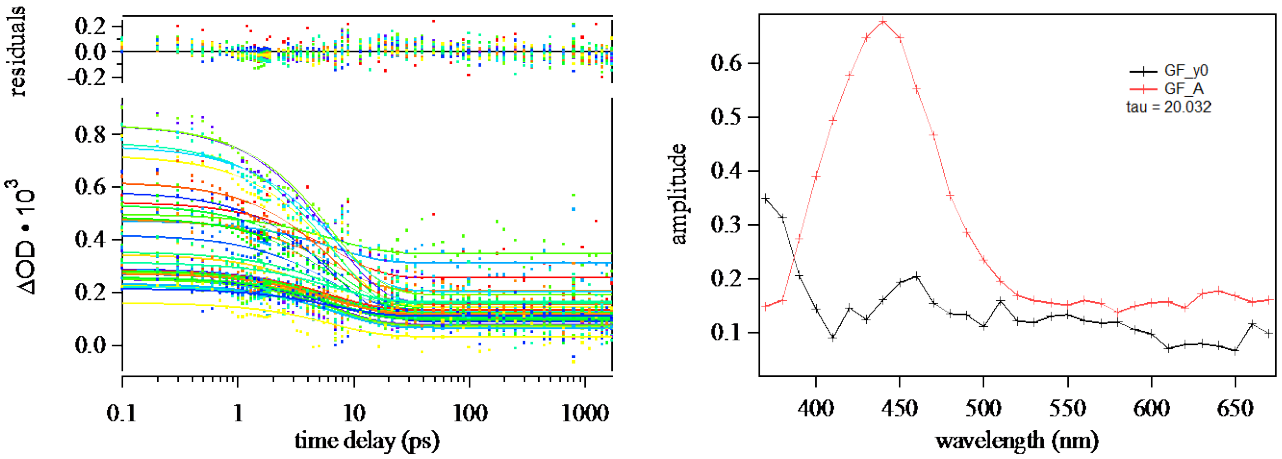

Figure S7. Results of global fitting observed TA spectra across all wavelengths for H_2DPA to an equation of the form; $\Delta OD_{(t)} = y_0 + A \exp^{-1/tau \times t}$, where tau represents the S_1 state lifetime, and y_0 the observed residual TA spectrum at long time delays (> 1.7 ns).

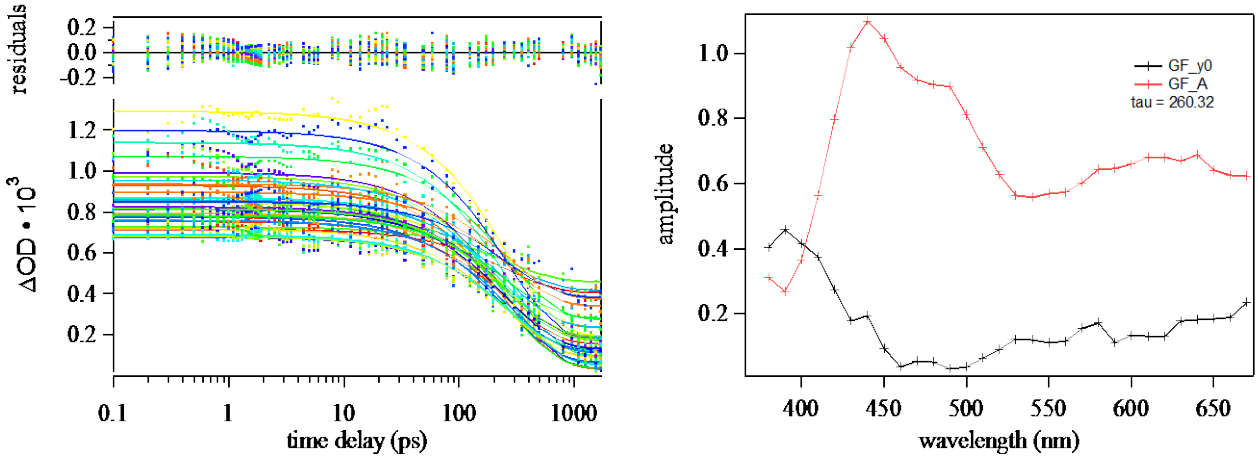

Figure S8. Results of global fitting observed TA spectra across all wavelengths for H_2PYZ to an equation of the form; $\Delta OD_{(t)} = y_0 + A \exp^{-1/tau \times t}$, where tau represents the S_1 state lifetime, and y_0 the observed residual TA spectrum at long time delays (> 1.7 ns).

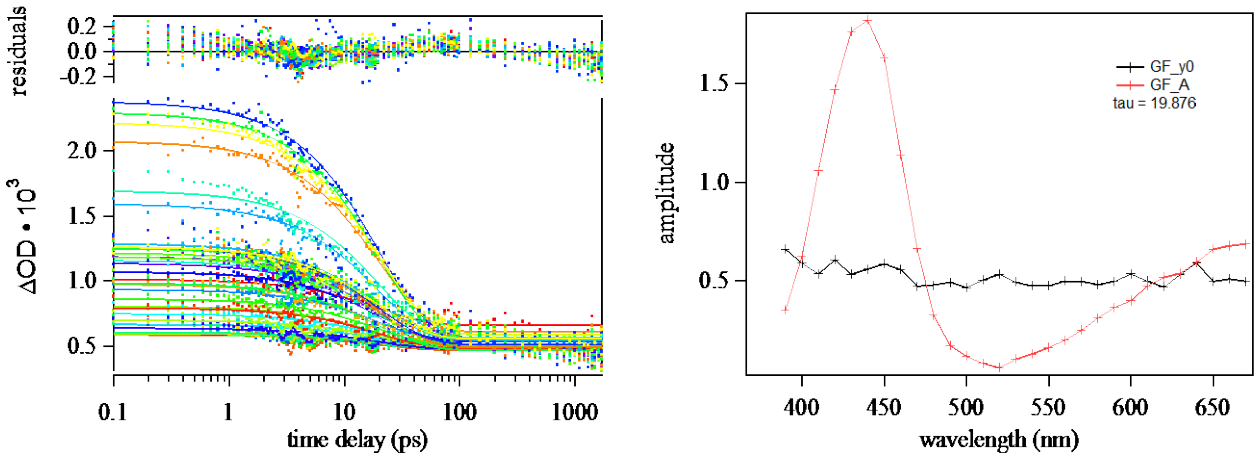

Figure S9. Results of global fitting observed TA spectra across all wavelengths for $[Gd(DPA)_3]^{3-}$ to an equation of the form; $\Delta OD_{(t)} = y_0 + A \exp^{-1/tau \times t}$, where tau represents the S_1 state lifetime, and y_0 the observed residual TA spectrum at long time delays (> 1.7 ns).

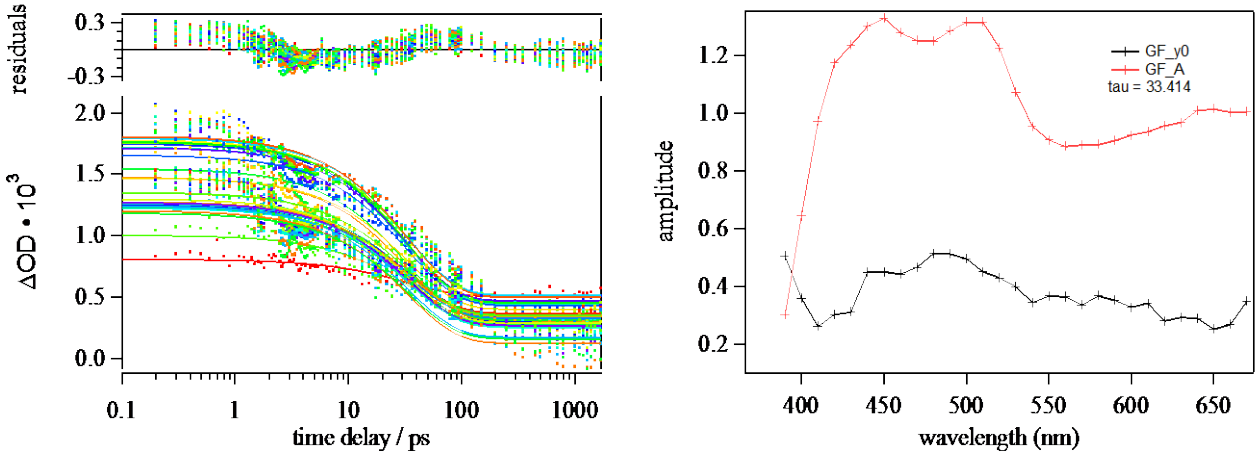

Figure S10. Results of global fitting observed TA spectra across all wavelengths for $[Gd(PYZ)_3]^{3-}$ to an equation of the form; $\Delta OD_{(t)} = y_0 + A \exp^{-1/tau \times t}$, where tau represents the S_1 state lifetime, and y_0 the observed residual TA spectrum at long time delays (> 1.7 ns).

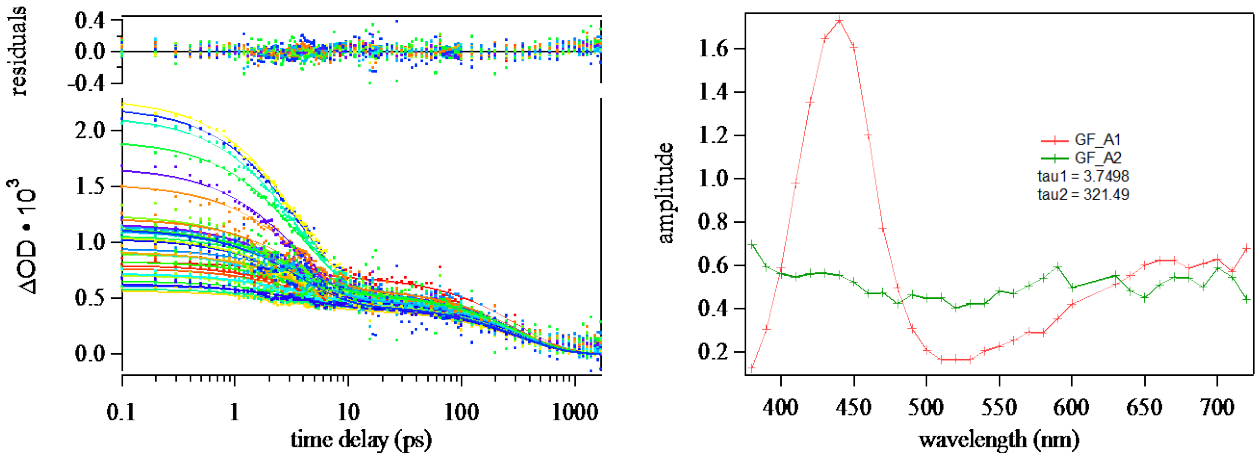

Figure S11. Results of global fitting observed TA spectra across all wavelengths for $[Eu(DPA)_3]^{3-}$ to an equation of the form; $\Delta OD_{(t)} = A1\ exp^{-1/tau1 \times t} + A2\ exp^{-1/tau2 \times t}$, where tau1 represents the S_1state lifetime, and tau2 represents the T_1 state lifetime.

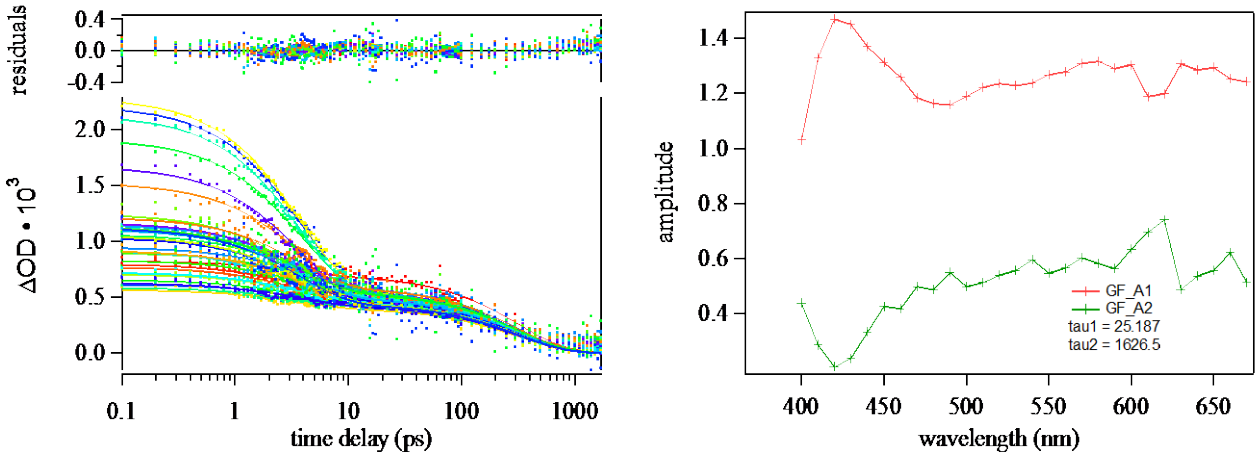

Figure S12. Results of global fitting observed TA spectra across all wavelengths for $[Eu(PYZ)_3]^{3-}$ to an equation of the form; $\Delta OD_{(t)} = A1\ exp^{-1/tau1 \times t} + A2\ exp^{-1/tau2 \times t}$, where tau1 represents the S_1 state lifetime, and tau2 represents the T_1 state lifetime.

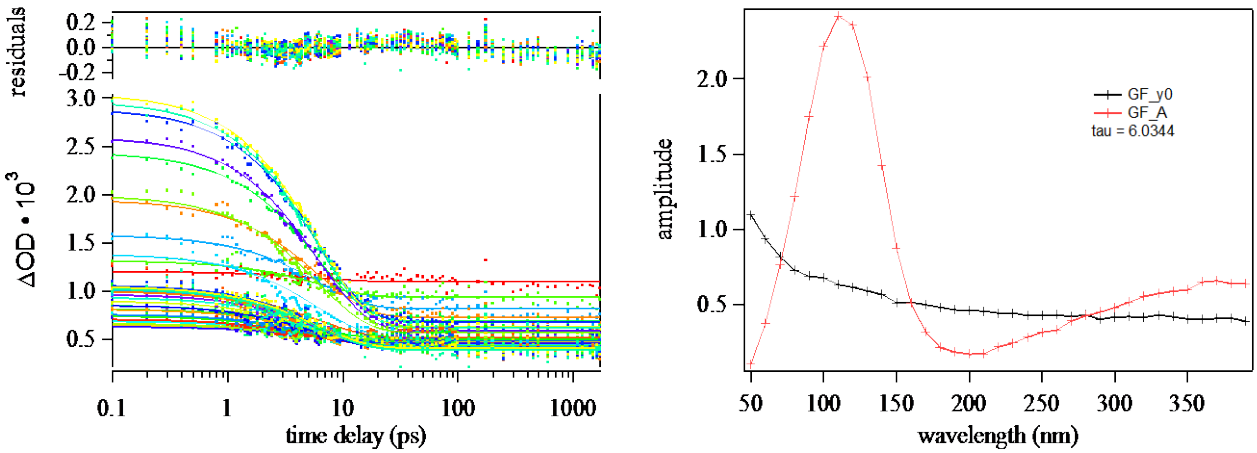

Figure S13. Results of global fitting observed TA spectra across all wavelengths for $[Yb(DPA)_3]^{3-}$ to an equation of the form; $\Delta OD_{(t)} = y_0 + A \exp^{-1/tau \times t}$, where tau represents the S_1 state lifetime, and y_0 the observed residual TA spectrum at long time delays (> 1.7 ns).

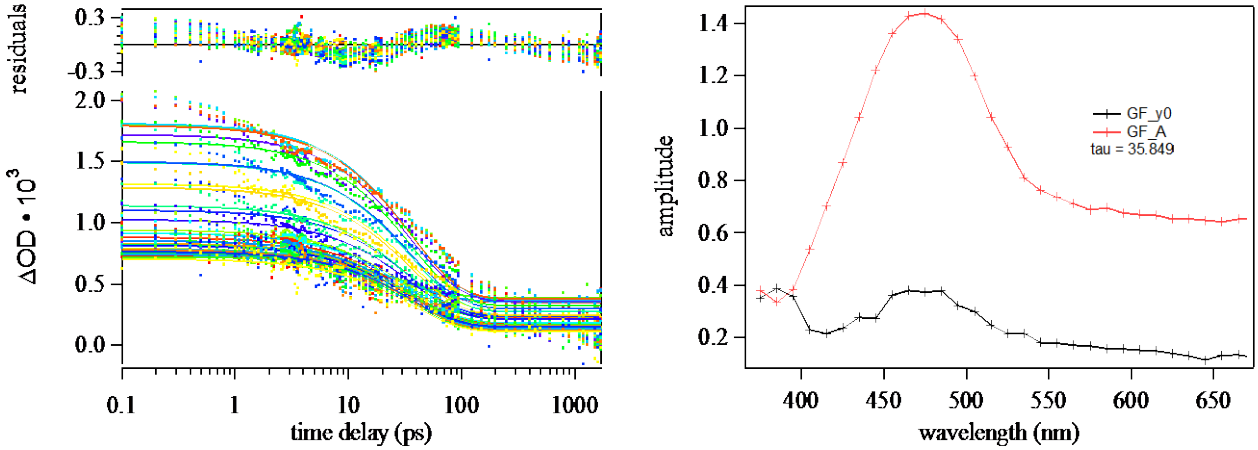

Figure S14. Results of global fitting observed TA spectra across all wavelengths for $[Yb(PYZ)_3]^{3-}$ to an equation of the form; $\Delta OD_{(t)} = y_0 + A \exp^{-1/tau \times t}$, where tau represents the S_1 state lifetime, and y_0 the observed residual TA spectrum at long time delays (> 1.7 ns).